Proceedings of 12th Asian Symposium on Visualization

Reynolds Number Effects on Wind Flows around Hemispherical Domes by Visualization Technique

Yuan-Lung Lo, Chung-Lin Fu, Chii-Ming Cheng
Department of Civil Engineering, Tamkang University, New Taipei City, Taiwan
Email: yllo@mail.tku.edu.tw

Abstract

In general, visualization experiment in a conventional boundary layer wind tunnel for buildings is a difficult task to carry out. This research intends to conduct the visualization experiment through the direct observation on the surrounding wind flow. The occurrence of flow separation along the surface is preliminarily observed. By high-speed camera, the location of the separation point moves forward to the downstream as the Reynolds number increases.

Keywords: Wind Tunnel, Hemispherical Domes, Reynolds Number, Separation

1. Introduction

A boundary layer forms when a fluid body passes a plate or a bluff body and is considered to be dominated by the fluid viscosity, bluff body's surface curvature, surface roughness, and Reynolds number effect. The fluid body moves from the upstream to downstream and once the pressure gradient on the surface cannot maintain the inertial force, the streamlines of fluid body separates from the surface in a certain angle. Such a phenomenon is called separation. Near the wall surface, due to the occurrence of the convection flow, the boundary layer becomes much thicker and the separation position is in general defined as the position where the wall pressure gradient or shear stress disappear. Researches have been published regarding the separation phenomenon of a boundary layer due to Reynolds number effect, especially on circular cylinders or spheres. For a hemisphere connected to the ground, the flow field along the surface will be even more complicated because of the ground surface roughness. Hence, the research target of a hemisphere is mainly for the building design and is usually immersed in turbulent flows. In this research, a visualization test of a hemispherical acrylic roof model is conduct in the wind tunnel. Through the observation of the surface flow movement, certain characteristics of the flow field are observed and discussed.

2. Experimental Setup

2.1. Wind Tunnel and Visualization Technique

Wind tunnel test and visualization technique were conduct in Wind Engineering Research Center, Tamkang University. The testing section of the wind tunnel is 18.0m in length, 3.2m in width, and 2.0m in height. A axial flow fan with diameter 2.2m is installed and provides wind flow with velocity 1.0m/sec ~ 15.0m/sec. A hemispherical acrylic model with the diameter 0.5m is manufactured on a thin plate, which is elevated above the ground surface of the wind tunnel to avoid the boundary layer effect of the ground. A laminar flow environment is then simulated for the subsequent wind tunnel tests. Visualization equipment of 2W argon ion laser manufactured by NEC Co. Ltd. is utilized for lighting source. Laser beam transmits through the optical fiber to a 1.5cm-diameter glass circular cylinder and radiates to fan-shaped laser sheet. The laser sheet is then reflected to the field over the acrylic model for wind flow observation.

In order to clearly observe the wind flow around the model, titanium tetrachloride is adopted as tracing material. Titanium tetrachloride generates smoke once got in touch with hydrogen oxide in the air. The smoke density is almost as heavy as the air so that the smoke will be stable for observation. Titanium tetrachloride is carefully smeared over the surface of the acrylic model to generate smoke. Then high-speed camera is setup to catch photos of the smoke movement over the acrylic model.

2.2. Wind Speed Measurement

In this research, not only the surface pressure of the acrylic model, but also wind velocity field in the downstream behind the model is measured. For the highly 3 dimensional feature of the downstream area, a 3D windspeed anemometer, Cobra Probe, which is produced by Turbulent Flow Co. Ltd., is utilized for the windspeed

measurement. Cobra Probe is a four-aperture sensor to measure the fluctuating wind speed comes from along-wind, lateral and vertical wind direction and the background static pressure. Mean wind speed, fluctuation wind speed, and wind speed spectrum. The measuring angle of the sensor is up to 45 degree, which is wider than a normal 2D hot wire anemometer.

3. Experimental Results

3.1. Visualization of Wind Flow Field

Figure 1 shows the side view of the smoke flow along the model surface under the flow condition of Reynolds number range from $7.4\times10^4 \sim 3.5\times10^5$. Wind flow direction is toward to the right so that the generating smoke by titanium tetrachloride moves along the surface to the downstream. Obvious difference is indicated under different Reynolds number. Figure 1(a) shows the flow status when Reynolds number is 7.4×10^4. It is clearly shown that the moving smoke in the upstream area is press close to the surface. Then a white tangential smoke line is form and stretched to the up-right direction around 80 degree, which is considered the separation phenomenon of wind flow. The separated smoke then forms vortices and dissipate in the downstream area. Figure 1(b) shows that the separation phenomenon occurs around 85 degree when the Reynolds number is increased to 1.4×10^5. Subsequent figures then show the same trend that the separation occurs downstream to 90 and 95 degree when the Reynolds numbers are 2.0×10^5 and 2.5×10^5 respectively. However, when the Reynolds number is increased to 3.0×10^5 and 3.5×10^5, obvious movement of separation is no longer indicated and the separation point is judged around 100 degree.

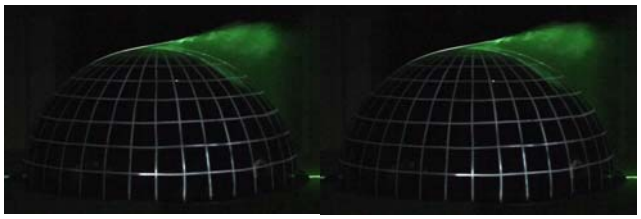

(a) 7.4×10^4 (b) 1.4×10^5

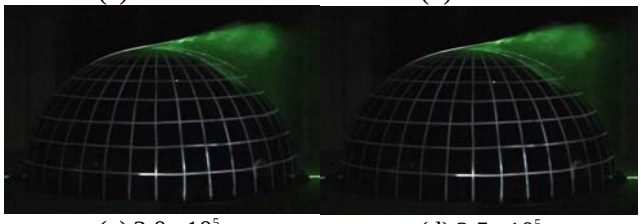

(c) 2.0×10^5 (d) 2.5×10^5

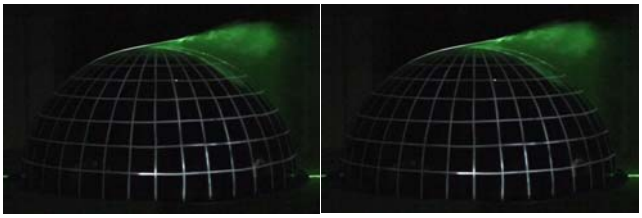

(e) 3.0×10^5 (f) 3.5×10^5

Figure 1 Side view of the generating smoke of the model surface ($Re = 7.4\times10^4 \sim 3.5\times10^5$)

Figure 2 shows the top view of the smoke movement on the model surface under Reynolds number $7.4\times10^4 \sim 3.5\times10^5$. The approaching wind direction is from the left-hand side to the right-hand side. Smoke generated by titanium tetrachloride moves from the windward area (left-hand side) to the leeward area (right-hand side) along the surface. From Figure 2(a), Reynolds number 7.4×10^4, titanium tetrachloride is smeared in the windward area around 30 degree and forms a white smoke belt. The generating smoke moves to the downstream and separates from the surface around 80 degree, where another white smoke belt is observed. In fact, the white smoke belt shown around the 80 degree is not fixed but slight moves back and forward. 80 degree is an empirical identification. Same features are indicated in Figure 2(b) and 2(c). The white smoke belt is observed respectively around 85 and 90 degree with 5-degree difference. However, in Figure 2(d) of Reynolds number 2.5×10^5, besides the white smoke belt keeps moving to the downstream, the belt itself becomes wider and the color slightly fades. Such wider belt is considered the occurrence of separation bubble empirically. Similarly, this bubble moves back and forward as previous cases. Figure 2(e) represents a more obvious separation bubble area around 100~115 degree under Reynolds number 3.0×10^5 and 105~120 degree for Figure 2(f) under Reynolds number 3.5×10^5.

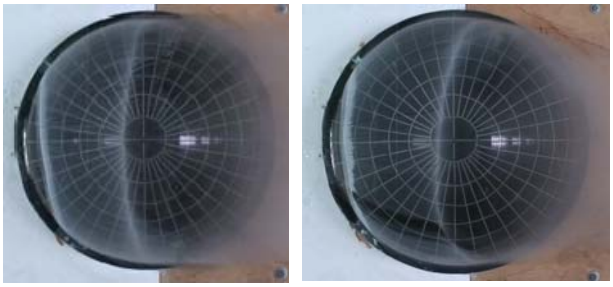

(a) 7.4×10^4 (b) 1.4×10^5

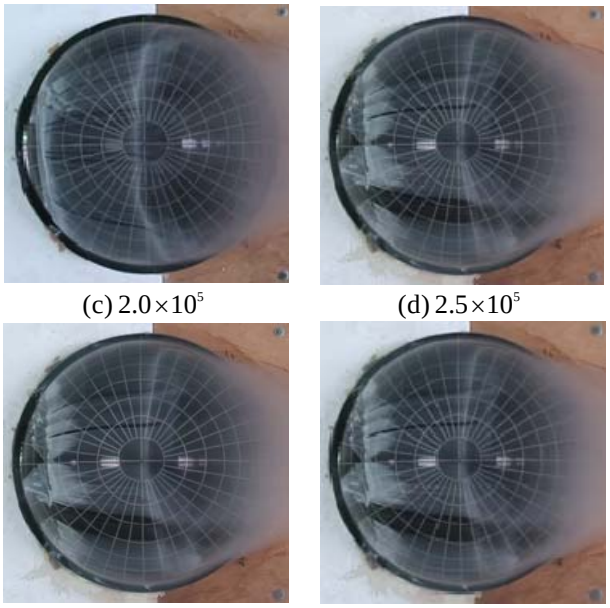

(c) 2.0×10^5 (d) 2.5×10^5

(e) 3.0×10^5 (f) 3.5×10^5

Figure 2 Side view of the generating smoke of the model surface ($Re = 7.4\times10^4 \sim 3.5\times10^5$)

From Figure 1 and 2 shown above, the separation point moves to the downstream as the increase of Reynolds number. When Reynolds number is less than 2.0×10^5, the separation bubble behind the separation point will directly dissipate to the downstream; the bubble then intermittently reattaches the model surface when Reynolds number is larger than 2.0×10^5. The bubble will completely reattach the model surface and then separate from the surface again when Reynolds number is larger than 3.0×10^5.

3.2. Wind Speed Field Measurement

In order to enhance the understanding of the wind velocity field over the model, 3D anemometer, Cobra Probe, is utilized to measure the wind velocities in the downstream area along the meridian line of the model roof. The measuring plane range is originated at the center of the hemispherical model and defined on the plane that passes the meridian line of the model, 35cm to the downstream and 30cm to the upstream. The measuring plane is meshed into orthogonal grids. Each grid has a $1.0\text{cm}\times1.0\text{cm}$ size and the right bottom corner of each grid is the measuring point. The measuring diagram is shown as Figure 3. For enormous measuring work, only Reynolds number equals to 2.0×10^5 and 3.0×10^5 cases are conduct.

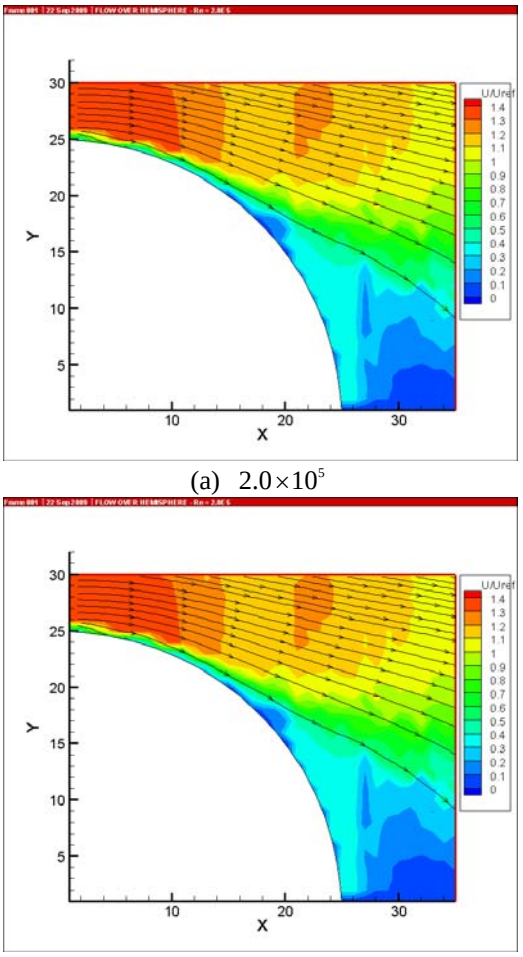

(a) 2.0×10^5

(b) 3.0×10^5

Figure 3 Contours of mean wind velocities and streamlines on the measuring plane passing the meridian line of the model

Figure 3 represents the contours of both cases indicating mean wind velocities; the white area is the model itself. For Reynolds number 2.0×10^5 in Figure 3(a), Wind flow is speed up at the model apex and observed the highest velocity. The reduced velocity is 1.4 at the apex and then decreased to 1.0 in the downstream area. Since the velocity at the model surface equals zero, the velocity, which forms the thin boundary layer, is varied dramatically. The boundary layer forms along the surface near the model top and stretches to the downstream. And then the boundary layer dissipates away and the separation of wind flow occurs. Similar observation can be indicated in Figure 3(b). However, with the increase of Reynolds number, the separation of wind flow is further to the downstream area.

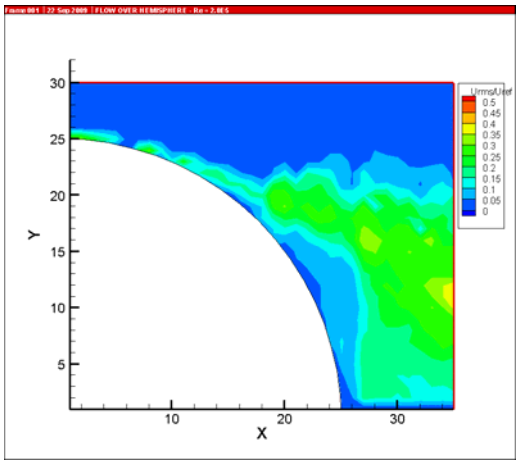

(a) 2.0×10^5

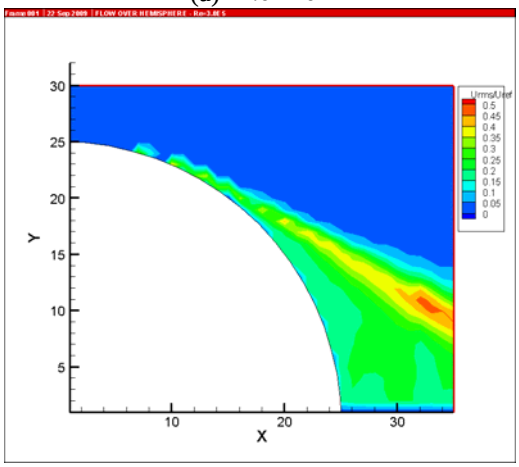

(b) 3.0×10^5

Figure 4 Contours of mean wind velocities on the measuring plane passing the meridian line of the model

Figure 4 represents the contour figures of fluctuating wind velocities. It is indicated in both figures that the velocity fluctuation is significant in the downstream area. For the case of Reynolds number 2.0×10^5, the significant fluctuating velocity area is wider than the case of 3.0×10^5 that concentrative contour is shown. Besides fluctuating wind velocities, vorticity distribution of the measuring area is also plotted into contours as shown in Figure 5. The definition of vorticity is

$$\omega_y = \frac{\partial W}{\partial X} - \frac{\partial U}{\partial Z}$$

where

U : along-wind (X-direction) wind velocity;
W : vertical (Z-direction) wind velocity;

The contour of vorticity is quite similar to the case of fluctuating wind velocities. Significant vorticities are indicated widely in the downstream area for the case of Reynolds number 2.0×10^5. On the other hand, condensed vorticity distribution is shown in the case of 3.0×10^5.

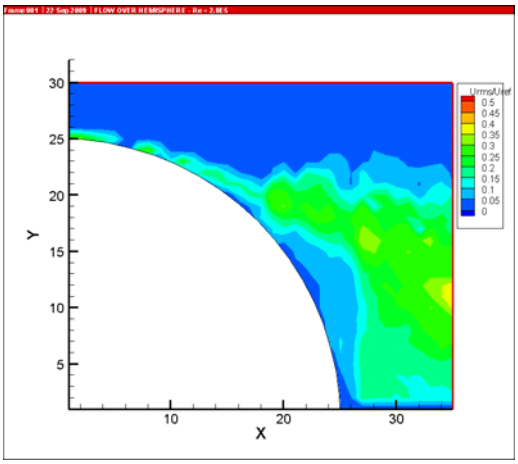

(a) 2.0×10^5

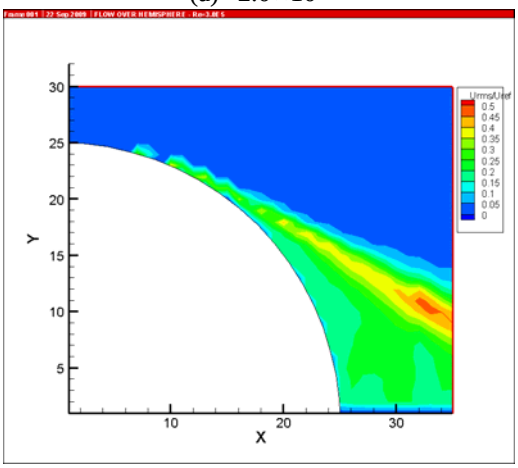

(b) 3.0×10^5

Figure 5 Contours of vorticity on the measuring plane passing the meridian line of the model

4. Conclusions

It is concluded from the above observations, wind flow approaches the model and then forms a thin boundary layer along the surface. When the Reynolds number is less than 2.0×10^5, separation of wind flow occurs at 85 degree; When the Reynolds number is larger than 3.0×10^5, the boundary layer turns to turbulences and the separation point moves to the downstream to form a separation bubble. Therefore the wake area is reduced to decrease largely the drag force at critical Reynolds numbers.

5. Acknowledgement

Acknowledgement is given to Prof. Cheng Lin in Dept. Civil Eng., National Chung Hsing University for his

invitation of attending of 12th Asian Symposium on Visualization and short laboratory tour for PIV measurement technique.

REFERENCES

[1] H. Schlichting, K. Gersten, Boundary Layer Theory, 8th Revised and Enlarged Edition, Springer-Verlag Berlin Heidelberg New York.

[2] F.J. Maher, Wind loads on basic dome shapes, 1965. J. Struct. Div. ASCE ST3, 219-228.

[3] N. Toy, W.D. Moss, E. Savory, 1983. Wind tunnel studies on a dome in turbulent boundary layers, J. Wind Eng. Ind. Aerodyn. 1, 201-212.

[4] T.J. Taylor, 1991. Wind pressures on a hemispherical dome, J. Wind Eng. Ind. Aerodyn. 40, 199-213.

[5] T.Ogawa, M. Nakayama, S. Murayama, Y. Sasaki, 1991. Characteristics of wind pressures on basic structures with curved surfaces and their response in turbulent flow, J. Wind Eng. Ind. Aerodyn. 38, 427-438.

[6] C.W. Letchford, P.P. Sarkar, 2000. Mean and fluctuating wind loads on rough and smooth parabolic domes, J. Wind Eng. Ind. Aerodyn. 88, 101–117.

[7] C. M. Cheng , C. L. Fu, 2010, “Characteristics of wind loads on a hemispherical dome in smooth flow and turbulent boundary layer flow”, Journal of Wind Engi-neering and Industrial Aerodynamics, 98, 328-344.

[8] C. M. Cheng , C. L. Fu, 2009, “REYNOLDS NUMBER EFFECTS ON HEMISPHERICAL DOMES IN SMOOTH FLOW”, The Seventh Asia-Pacific Conference on Wind Engineering, November 8-12, 2009, Taipei, Taiwan, 523-526.